Distribution of Relaxation Times Analysis of High-Temperature PEM Fuel Cell Impedance Spectra

CrossMark

Alexandra Weiß[a], Stefan Schindler[a], Samuele Galbiati[a], Michael A. Danzer[b,c], Roswitha Zeis[a,d,*]

[a] Karlsruhe Institute of Technology, Helmholtz Institute Ulm, Helmholtzstraße 11, 89081 Ulm, Germany
[b] Chair of Electrical Energy Systems, University of Bayreuth, Universitätsstraße 30, 95447 Bayreuth, Germany
[c] Zentrum für Sonnenenergie- und Wasserstoff-Forschung Baden-Württemberg, Lise-Meitner-Str. 24, 89081 Ulm, Germany
[d] Karlsruhe Institute of Technology, Institute of Physical Chemistry, Fritz-Haber-Weg 2, 76131 Karlsruhe, Germany

ABSTRACT

In this study, Distribution of Relaxation Times (DRT) was successfully demonstrated in the analysis of the impedance spectra of High-Temperature Polymer Electrolyte Membrane Fuel Cells (HT-PEMFC) doped with phosphoric acid. Electrochemical impedance spectroscopy (EIS) was performed and the quality of the recorded spectra was verified by Kramers-Kronig relations. DRT was then applied to the measured spectra and polarization losses were separated on the basis of their typical time constants. The main features of the distribution function were assigned to the cell's polarization processes by selecting appropriate experimental conditions. DRT can be used to identify individual internal HT-PEMFC fuel cell phenomena without any a-priori knowledge about the physics of the system. This method has the potential to further improve EIS spectra interpretation with either equivalent circuits or physical models.
© 2017 The Authors. Published by Elsevier Ltd. This is an open access article under the CC BY-NC-ND license (http://creativecommons.org/licenses/by-nc-nd/4.0/).

1. Introduction

High-temperature polymer electrolyte membrane fuel cells (HT-PEMFCs) using Polybenzimidazole (PBI) membranes doped with phosphoric acid can operate in the temperature range between 140 °C and 200 °C [1–3]. HT-PEMFCs are one of the most promising systems for distributed cogeneration of electricity and heat on a small scale using hydrogen as fuel. Operating at elevated temperatures provides enhanced tolerance against impurities ([CO] ∼ 3 %) and profitable heat recovery [4]. There is no need for liquid water within the cell, where phosphoric acid is used as proton conductor. As a result, dry reactants can be used and water management in the system is simplified compared with low-temperature fuel cells. However, HT-PEMFCs tend to show low performance compared with low-temperature fuel cells. Therefore it is important to identify polarization losses by a suitable in-situ technique, such as electrochemical impedance spectroscopy [5–8]. EIS can be recorded without altering the working conditions of the fuel cell and can thus be used to determine the impact of different parameters (e.g. reactants stoichiometry, current density,

temperature) on cell operation. Three features are usually visible in HT-PEMFC impedance spectra and are typically attributed to anode phenomena and membrane resistivity (high frequency arc > 100 Hz), kinetics (intermediate frequency arc ≈ 10-100 Hz), and mass transport (low frequency arc ≈ 1 Hz) [9–11].

Although a general agreement about these associations is shared in the literature, a clear separation of the features and their direct assignment to single-cell polarization losses is not trivial. In particular, the shape and size of the arcs, their distribution in the frequency domain, and their overlap can change significantly at different operating conditions.

Impedance spectra are usually interpreted using an equivalent circuit model (ECM) [12,13]. In this approach, physical phenomena taking place in the fuel cell during operation are represented by equivalent electrical elements. The value of the single equivalent electrical elements is obtained by the fitting of the measured impedance data by means of mathematical algorithms. The analysis of impedance spectra of HT-PEMFC by ECM has been extensively reported in the literature. ECM approaches have been applied to the study of several aspects of HT-PEMFC such as MEA activation and acid redistribution upon startup [14–17], resistance variation upon membrane hydration [18,19], electrode composition and cell components [10,11,20–24], cell operating parameters [9,11,22], presence of pollutants in the fuel stream [25–32], and cell

* Corresponding author.
  E-mail address: roswitha.zeis@kit.edu (R. Zeis).

degradation over time [33–36]. Precious information was obtained by all these studies.

ECM is a powerful instrument in EIS interpretation since it can be used to extract trends without implementing more complex physical models [7,37,38]. But the appropriate use of ECM to fit impedance data relies on a priori knowledge about the system since it requires a suitable model structure that represents the physical processes occurring in the cell. Conversely, if there is little a priori knowledge about the system, the choice of an appropriate model structure can become a difficult task. Furthermore, for the same electrochemical system, different models might be needed to accurately reproduce the system behavior when the operating conditions change [39].

A complementary approach that supports the development of ECM models is the analysis of the Distribution of Relaxation Times. Originally introduced for the impedance analysis of solid oxide fuel cells [40] and lithium-ion batteries [41,42], DRT can be used for process identification in complex electrochemical systems, where resistive-capacitive (R//C) features are dominant [43]. This methodology does not require the definition of a specifically-designed equivalent circuit, thus minimizing the need for "a priori" assumptions in the study of an electrochemical system. In this approach, the system is modeled by a quasi-infinite series of R//C – elements without specific considerations about the occurring phenomena. The quasi-infinite network of R//C – elements is applied to the fitting of the impedance spectrum. The individual processes are separated on the basis of their typical time constants, derived from the associated R//C – elements. This approach requires only little computational effort due to its simplicity. DRT allows us to bypass ambiguous EC modelling and analyze spectra "model-free", without pre-assumptions. DRT can be used to separate different polarization losses and thus help reconstruct a physical model for the ECM analysis.

In this work, DRT was applied to the study of impedance spectra of PEM fuel cells using Polybenzimidazole (PBI) membranes doped with phosphoric acid. Well defined experimental conditions (gas-composition and stoichiometry, current density and certain operating modes) were selected in order to facilitate the identification of the fuel cell internal processes on the basis of their characteristic time constants. This methodology revealed the association of typical frequencies in the DRT spectrum to cell physical phenomena.

2. Experimental

2.1. Cell Assembly

In this study Membrane Electrode Assemblies (MEA's) with an active surface area of 4 cm^2 were prepared. Commercial Polybenzimidazole (PBI) membranes (Dapazol®, Danish Power Systems-DPS®) [44] were doped by immersion in concentrated phosphoric acid (85 %wt. VWR Chemicals®) at room temperature ($T \approx 20$ °C) for approximately 15 days.

Gas diffusion electrodes were fabricated by spray-coating in our laboratory. A catalyst ink was prepared using a commercial supported catalyst powder (20 % Pt/C by Heraeus®), isopropanol and water (1:1 by volume) as solvents and a PTFE suspension (60 % wt. 3 M®) as binder. The solid weight fraction of the ink was no more than 5 % to allow spray-coating [10,23,45–47].

The catalyst ink was sprayed directly onto a Gas Diffusion Layer provided with a microporous layer (GDL, H2315-C2 by Freudenberg®). Multiple layers of the catalyst ink were deposited until the desired loading was reached (1 mg$_{Pt}$/cm^2 for both anode and cathode). During this process the loading was periodically determined by weighing. The evaporation of the solvent was

accelerated by placing the GDL on a heating plate ($T = 80$ °C) during spraying [10,23,45–47].

The fuel cell assembly was designed and built in-house and consisted of metallic bipolar plates with single serpentine flow-fields (channel cross section: 1 mm x 1 mm), aluminum plates equipped with heating pads and temperature sensors, gaskets (PTFE foil; thickness 200 μm) and subgaskets (PEEK foil; thickness 25 μm) [10,23,45,46].

2.2. Measurement techniques

Polarization curves were measured in galvanostatic mode with an external load applying the required current. During operation the anode and the cathode were fed with hydrogen ($\lambda_{H2} = 1.8$) and air ($\lambda_{Air} = 2.5$), respectively. The temperature ($T = 160$ °C) and the stoichiometry were kept constant. Polarization curves were recorded by increasing the current stepwise from 0 mA cm^{-2} (open circuit) up to 800 mA cm^{-2}. The flow rates were adjusted according to the required current in order to ensure constant stoichiometry (due to flow controller limitations the flowrates are kept constant below 200 mA cm^{-2}). The measurements were stopped if the voltage decreased below 300 mV [10,23,45,46]. Additionally impedance spectra were recorded at each condition in galvanostatic mode using a Zahner® Zennium potentiostat. Current load was applied using a Zahner Zennium workstation (Zahner, Zennium) [10]. To exclude any electrical interference specifically designed shielded, twisted pair cables were used to connect the potentiostat to the fuel cell. The spectra were taken in a frequency range of 100 kHz –100 mHz with a perturbation amplitude of 100 mA at 10 measurement points per decade. To exclude cell drift, the cell was stabilized for ~30 min before each measurement. More experiments were carried out by operating the fuel cell with pure oxygen at the cathode, the oxygen volumetric flow rate was set equal to the air volumetric flow rate at each measured point (Fig. 1). "Hydrogen pumping" experiments were performed supplying the cell with hydrogen to both anode ($\lambda = 1.8$) and cathode (30 Nmlmin^{-1}) compartments. In this case, hydrogen was oxidized at the anode, and protons moved through the ionomer membrane and reached the cathode where they were reduced to hydrogen [48]. Therefore the oxygen reduction reaction (ORR) did not take place in the "hydrogen pumping" mode (Fig. 1c). Hydrogen pumping experiments were conducted with humidified gases ($T_{sat.} = 40$ °C) to avoid drifts in membrane resistivity over time. The effect of humidification on the impedance measurements was negligible since the relative humidity in the cell was below 2 %.

2.3. Analysis techniques

2.3.1. Kramers-Kronig Validity Test

Good data quality and high signal-to-noise ratio are critical for this study. Even a small measurement noise can lead to inaccurate assignment of electrochemical processes and misinterpretations in modelling. Therefore the validity of the measured impedance data needs to be certified before further processing. An often-used method for this purpose is the Kramers-Kronig transform of the impedance data set. If the recorded impedance data satisfies the conditions of linearity and time-invariance, the real and imaginary parts have the following constraints (Eq. (1)):

$$Z^{'}(\omega) = Z^{'}(\infty) + \frac{2}{\pi} \int_0^\infty \frac{xZ^{''}(x) - \omega Z^{''}(\omega)}{x^2 - \omega^2} dx$$

$$Z^{''}(\omega) = -\frac{2\omega}{\pi} \int_0^\infty \frac{Z^{'}(x) - \omega Z^{'}(\omega)}{x^2 - \omega^2} dx \qquad (1)$$
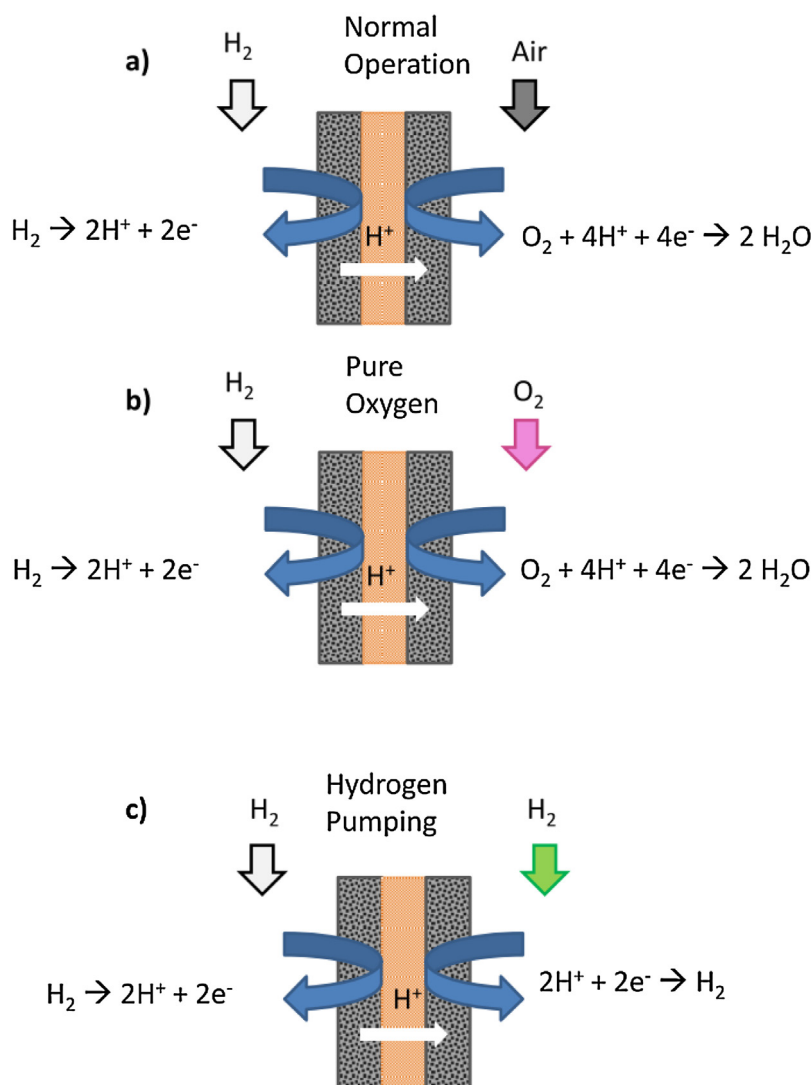
Fig. 1. Schematic representation of the investigated experimental conditions: a) normal operation H_2/Air, b) normal operation with H_2/O_2, c) hydrogen pumping H_2/H_2.

where $Z''(\omega)$ represents the imaginary part of the impedance, $Z'(\omega)$ the real part and ω the angular frequency. It is not possible to solve the semi-infinite integral in Eq. (1) analytically. For practical applications the validity test is altered in a way that a Kramers-Kronig transform compliant measurement model is fitted to the measurement data and the relative residuals are considered (Eq. (2)) [5]:

$$\Delta_{\text{Re}}(\omega) = \frac{Z'(\omega) - \hat{Z}'(\omega)}{|Z(\omega)|}$$
$$\Delta_{\text{Im}}(\omega) = \frac{Z''(\omega) - \hat{Z}''(\omega)}{|Z(\omega)|}$$

(2)

where $|Z(\omega)|$ represents the absolute measured impedance at a given ω and $\hat{Z}(\omega)$ the model impedance. If the relative residuals in Eq. (2) are below 1%, the impedance data is assumed to fulfill the Kramers-Kronig relation. For this study, a linear Kramers-Kronig test based on [49] was applied to every impedance data set measured throughout our experimental activity.

2.3.2. Distribution of Relaxation Times

DRT can be used to represent the impedance by an infinite number of infinitesimal differential RC-elements [50]. By applying

DRT each electrochemical process is resolved by its intrinsic time constant. The magnitude of each process is assigned as a specific share of the overall polarization resistance. A distribution of the magnitude of the single processes in the frequency domain can be obtained. In Eq. (3) the relation between the distribution function $g(\tau)$ and the complex impedance $Z(\omega)$ is shown:

$$Z(\omega) = R_0 + R_{pol} \int_0^\infty \frac{g(\tau)}{1 + j\omega\tau} d\tau$$

(3)

The boundary condition for Eq. (3) is expressed by Eq. (4):

$$\int_0^\infty g(\tau) d\tau = 1$$

(4)

In Eq. (3) R_{pol} represents the overall polarization resistance of the fuel cell and R_0 the purely ohmic one. The time constant of a single RC-element is designated by $\tau = RC$, the fraction of the overall polarization resistance with relaxation times between τ and $\tau + d\tau$ is indicated by the term $\frac{g(\tau)}{1+j\omega\tau} d\tau$. The boundary condition in Eq. (4) states that the area below the distribution function equals one. This means that the integral of the polarization resistances of all the single phenomena corresponds to R_{pol}. Typically, if a measured impedance spectrum is used for the calculation, the distribution

function is discretized on a limited amount of time constants (Eq. (5), in our study we used 90 logarithmically distributed time constants in the frequency range of 100 kHz -100 mHz).

$$Z(\omega) = R_0 + R_{pol} \sum_{k=1}^{N} \frac{g_k}{1 + j\omega\tau_k} \qquad (5)$$

Eq. (5) Tikhonov cannot be solved analytically. To stabilize the numerical solution of the problem, Tikhonov regularization can be used [51]. The regularization is based on extension of the cost function by a term accounting for the smoothness of the solution [52]. The level of regularization is determined by a regularization parameter. The shape of features in the distribution function highly depends on the value of the regularization parameter: High values may result in features not clearly distinguishable, whereas low values can cause erroneous oscillations not related to the physicochemical processes of the system. In our study, we have carefully pre-evaluated the choice of the regularization parameter to obtain meaningful distribution functions for the given imped-ance data. It turned out that the value of $1 \cdot 10{-}5$ has been a meaningful compromise between the amount of indicated features and the obtained residuals. As already mentioned, g_k represents the relative share of each τ_k on the overall polarization resistance. Sometimes, it is helpful to account for the absolute resistance distribution instead, particularly if the impedance characteristics are compared with the information in the Nyquist plane. In this case, g_k has to be scaled according to:

$$h_k = R_{pol} \cdot g_k \qquad (6)$$

3. Results and Discussion

3.1. Validity of measurement data

As introduced in Section 2, application of DRT necessitates an outstanding measurement quality. Therefore, every measured spectra presented in the following evaluation has been validated
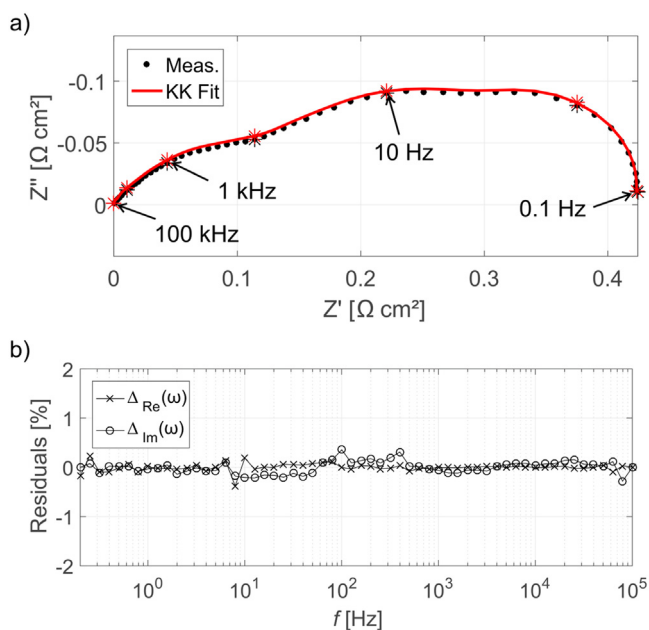
by Kramers-Kronig relations before applying DRT calculations [53]. In Fig. 2 a) and 2b) typical impedance spectrum for a HT-PEFMC and the corresponding Kramers-Kronig residuals are plotted. The residuals are less than 0.5 % for the whole frequency range. These considerably small residuals are taken as a confirmation of Kramers-Kronig validity and further processing is justified.

3.2. Assignment of the DRT function peaks

3.2.1. Fuel cell operation $-$ H_2/Air

The impedance spectrum measured during HT-PEMFC opera-tion in H_2/Air flows ($T = 160\,°C$, $\lambda_{H2} = 1,8$, $\lambda_{Air} = 2.5$, $j = 300\,mA\,cm^{-2}$) is depicted in Fig. 3 a). The impedance spectrum only exhibits three main features or discernable arcs at low (0.1–5 Hz), medium (5–100 Hz) and high frequencies (>100 Hz). The DRT spectrum obtained by the analysis of the shown EIS data is shown in Fig. 3 b).

The DRT analysis reveals seven distinct peaks: one main contribution at low frequency (**P1** -1 Hz), another main contribution at medium frequency (**P2**–30 Hz), followed by five distinct but less pronounced peaks (**P3-7-** over 50 Hz). Two main advantages are evident in the DRT analysis. First, the individual phenomena are displayed clearly by distinct peaks. Second, the high frequency arc in the impedance spectrum is divided into several peaks in the DRT spectrum. This points towards the presence of multiple distinct phenomena with multiple time scales, which are convoluted in the corresponding Nyquist plot.

In the following, experimental parameters were varied systematically to identify individual processes.

3.2.2. Fuel cell operation $-$ H_2/O_2

To exclude or at least minimize the mass transport losses, the cell was operated with pure oxygen ($\lambda_{O2} = 10$) instead of air (Fig. 4). Oxygen diffusion in the gas phase can be neglected when pure oxygen with high stoichiometry is used [7,54,55]. As revealed by the Nyquist plot, when the cell was operated with pure oxygen instead of air, the overall impedance decreased (Fig. 4 a). In
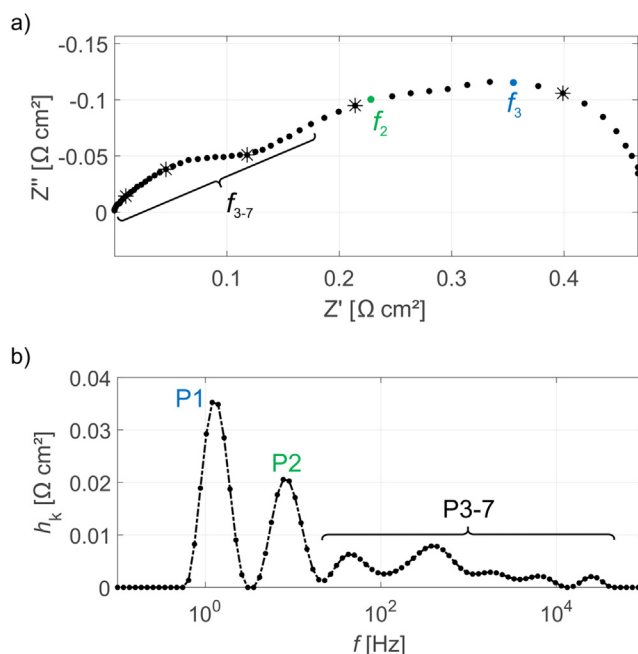

Fig. 2. (a) EIS spectra recorded at $T = 160\,°C$, $j = 300\,mA\,cm^{-2}$, $\lambda_{H2} = 1.8$, $\lambda_{air} = 2.5$ and (b) computational residuals of Kramers-Kronig reconstruction as a function of frequency. With the * symbol dimensions of frequencies are indicated. For comparison, R_0 has be subtracted in all the shown EIS spectra, therefore the intercept with the real axis is at 0.

Fig. 3. Impedance spectra (a) for a HT-PEMFC operated at $T = 160\,°C$, $j = 300\,mA\,cm^{-2}$, $\lambda_{H2} = 1.8$, $\lambda_{Air} = 2.5$ and the corresponding DRT plot (b). Seven distinct peaks are visible, indicating seven different physical phenomena.
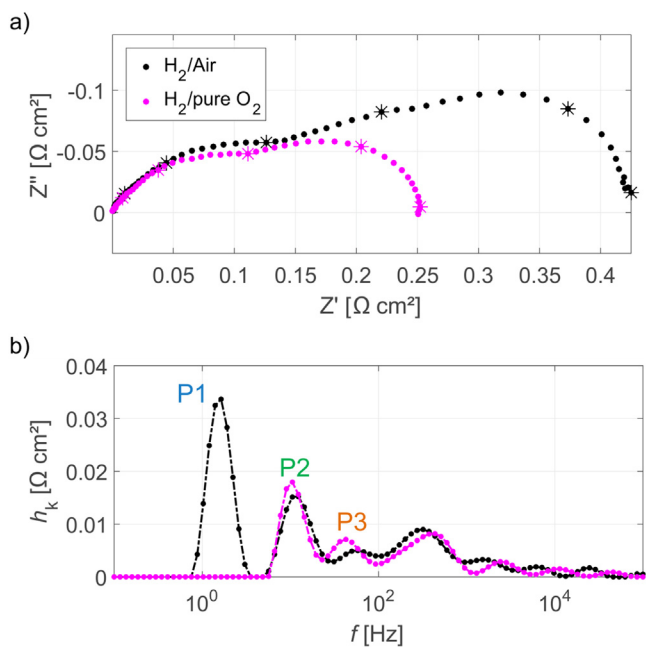
Fig. 4. Impedance spectra (a) and the corresponding DRT plot (b) for a HT-PEMFC operated with pure oxygen and $T = 160\,°C$, $j = 300\,mA\,cm^{-2}$, $\lambda_{H2} = 1.8$, $\lambda_{O2} = 10$ (pink data). Data of regular cell operation are also included (black data). The peak P1 located at 1 Hz is absent and can therefore be assigned to mass transport related process.

Fig. 5. Impedance spectra (a) and the corresponding DRT plot (b) for a HT-PEMFC operated in hydrogen pumping mode at $T = 160\,°C$, $j = 300\,mA\,cm^{-2}$, $\lambda_{H2} = 1.8$, $\lambda_{H2,}$ Cathode = 15 mL min^{-1}(green data). Data of regular cell operation are also included (black data). In addition to P1, the two peaks P2 and P3 at median frequencies are also absent and are assigned to ORR related processes.

particular, the low frequency part of the impedance spectrum ($\sim$ Hz) diminished. By applying the DRT analysis to the impedance data shown in Fig. 4 a, an equivalent DRT spectrum is obtained (Fig. 4 b-pink line). For comparison, the DRT spectrum corresponding to normal fuel cell operation in H₂/Air is also reported in the same figure (Fig. 4 b-black line). Note the peak located at 1 Hz (**P1**) completely disappears when pure O₂ is used instead of air, whereas the other peaks are only slightly affected. The concentration of O₂ is higher in this experimental condition, and therefore mass transport losses can be neglected. Locally resolved impedance spectra measured by Schneider et al. revealed that despite through plane mass transport losses, the depletion of oxygen down the flow field distributor as well as below the ribs are both contributing to the mass transport induced polarization losses [56]. Since the impedance measured in our study represents the impedance of the whole fuel cell, it is not possible to distinguish between in-plane and through plane mass transport losses. Therefore further experiments with locally resolved impedance spectra would be necessary. However, the missing peak in the DRT spectrum at 1 Hz is clearly related to cathode mass transport processes occurring at the characteristic frequency of 1 Hz. This result unequivocally proves that the third arc of the impedance spectrum at low frequencies is associated with mass transport generally, including both in-plane and through plane losses.

DRT reveals that mass transport losses are completely absent when pure oxygen is used, whereas an analysis of the Nyquist plot could not determine whether the mass transport related arc vanishes or if it is just weakened and hidden in another feature. DRT not only ultimately confirms that mass transport occurs at $\sim$ 1 Hz, but also separates processes which overlap in the Nyquist plane.

3.2.3. Hydrogen pumping – H₂/H₂

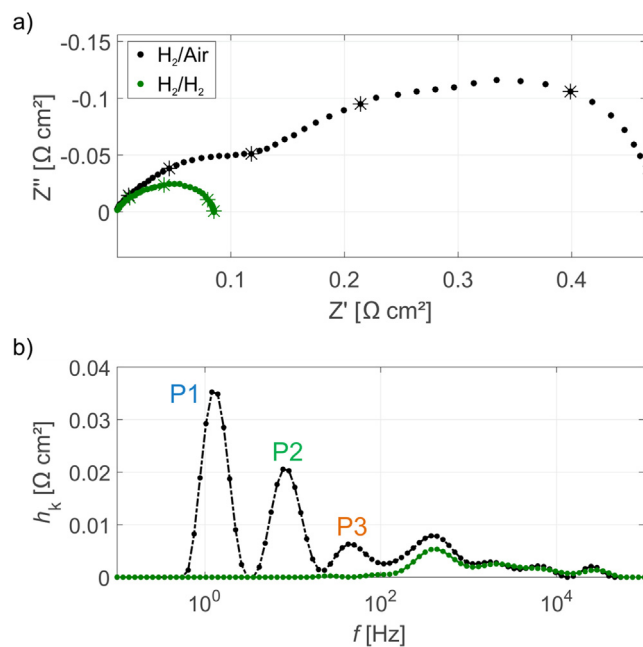As already mentioned, the cell was operated in "hydrogen pumping" mode by supplying hydrogen on both anode and

cathode compartments. In this condition oxygen is absent and no oxygen reduction reaction takes place within the cell [48].

Fig. 5 a) shows the impedance measured during "hydrogen pumping" (green line), compared with the impedance recorded during normal operation (black line). Only one of the original three half circles is still present when the HT-PEMFC is operated as hydrogen pump, furthermore the overall impedance signature is small compared with the one measured during regular cell operation in H₂/Air. The associated DRT distribution function is depicted in Fig. 5 b). In the distribution function related to the pumping experiment in H₂/H₂ streams (green line) **P1** to **P3** completely vanished, whereas **P4** slightly decreased. The peaks at high frequencies (**P5–P7**) are similar for both normal operation and hydrogen pumping. **P1** has been previously assigned to mass transfer processes (section: operation in H₂/O₂), such a peak is not present anymore when proton pumping is carried out in H₂/H₂ streams. In this case, hydrogen is recombined at the cathode side of the cell where a hydrogen stream is flowing. Therefore no mass transport induced by a concentration difference can take place. Therefore the disappearance of **P1** clarifies that mass transport losses are bound to the cathodic half-cell.

During the pumping experiment the ORR does not take place and the disappearance of **P2** and **P3** proves that these processes occurring at medium frequencies can be successfully correlated to oxygen reduction reaction related processes. So far it is assumed that at least one of both features is directly linked to the charge transfer kinetics of the ORR, whereas the other one can be interpreted by several different approaches: the ORR exhibits a complex multistep process, an additional surface species is formed [57] or phosphoric acid anions are adsorbed on the surface [58]. Limited by the measurement setup it's hard to distinguish which additional phenomenon is actually occurring and further experiments are necessary to clarify it. However, usually the feature correlated with the cathode is assumed to consist of a single process represented by a single arc in the Nyquist plot. By means of DRT we could show that the cathode related polarization loss

comprises two distinct features, which are associated with two separate time constants. This has not been observed in the Nyquist plane before, and it is new in the impedance analysis of HT-PEMFCs.

Since the process **P4** occurring at $\sim 200\,Hz$ is only slightly affected during hydrogen pumping and unaffected during the operation with pure oxygen, it could be associated with either charge transfer kinetics of the HOR, proton conduction losses, or a superposition of both. Further work will be carried out to confirm the assignment.

In summary, DRT has revealed that there are more than three processes contributing to the impedance of a HT-PEMFC (Fig. 6). By using pure oxygen the peak **P1** located at 1 Hz was associated with mass transport, which completely vanishes in the case of supplying oxygen or hydrogen to the cathode. The so far assumed one cathode related feature actually consists of two separate processes (**P2** and **P3**) occurring at different medium frequencies. Moreover, there are multiple processes contributing to the high frequency part of the impedance (**P4–P7**), and they presumably represent anode and proton conduction related phenomena.

3.3. DRT Analysis of parameter variation during cell operation

3.3.1. Cathode stoichiometry

To investigate the impact of cathode stoichiometry variation during operation by means of DRT, impedance was measured at different cathode stoichiometry ($\lambda_{Air} = 1.5$, 2.5 and 4.0) (Fig. 7). The other parameters like temperature ($T = 160\,°C$), anode stoichiometry ($\lambda_{H2} = 1.8$) and current ($j = 300\,mA\,cm^{-2}$) were kept constant.

In Fig. 7 a) the polarization curves under different conditions are plotted. The performance is initially almost constant over a wide range of current densities ($< 200\,mA\,cm^{-2}$) regardless of the air stoichiometry. At current densities beyond $300\,mA\,cm^{-2}$ the voltage decreases by decreasing λ_{Air}; which can be explained by a depletion of oxygen. The consumption of oxygen is larger at higher currents and an undersupply of oxygen at, especially below the
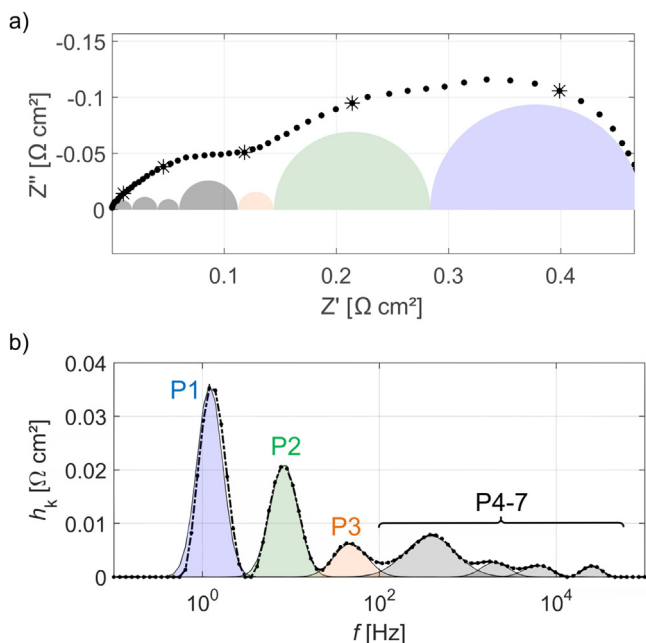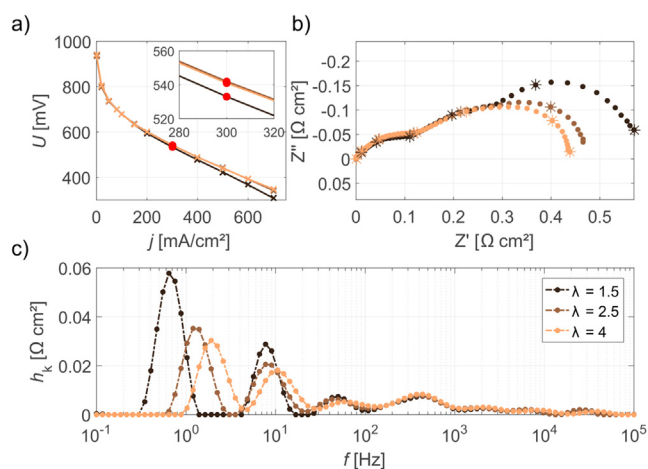

Fig. 7. Impact of cathode stoichiometry variation on HT-PEMFC polarization losses. (a) Polarization curves, (b) impedance and (c) DRT plots at different cathode stoichiometries ($T = 160\,°C$, $j = 300\,mA\,cm^{-2}$, $\lambda_{H2} = 1.8$).

ribs, is more likely to happen, therefore mass transport induced polarization losses are more pronounced at higher current densities [18,56].

The Nyquist plot reveals the three typical features at low (0.1–5 Hz), medium (5–100 Hz) and high frequencies (>100 Hz). Decreasing λ_{air} evidently increases the low frequency arc, most pronounced for $\lambda_{air} = 1.5$ (black curve), but leaves the high and the medium frequency arcs unaffected.

Analysis by means of DRT (Fig. 7 c) reveals again seven distinct peaks (**P1-P7**) within the measured frequency range [53]. **P1** is reduced and the frequency is shifted by an increase of λ_{Air}, whereas **P2** is only reduced. A small but still visible change is apparent for **P3**. The peaks located at higher frequencies (**P4–P7**) are unaffected by the stoichiometry variation. This confirms that besides mass transport the ORR related processes are also influenced by λ_{Air} [9].

The observed asymptotically decrease of **P1** with an increase of λ_{air} is in good agreement with the assignment of **P1** to mass transport processes. Reducing the stoichiometry of air causes a decrease in the average concentration of oxygen in the cathode flow field, and therefore mass transport losses are enhanced. This observation was also confirmed by the measured EIS spectra, where the arc at low frequency is more pronounced at low λ_{Air}. However, there is only a small decrease of **P1** observed, when the stoichiometry is further increased from 2.5 up to 4. This suggests that the active layer is progressively saturated with oxygen. Therefore, a further increase of λ_{Air} from 2.5 to 4 does not change mass transport losses significantly. This also explains the trends observed during operation with pure oxygen.

The second process (**P2**) and the third process (**P3**) occurring at around $\sim 10\,Hz$ and $\sim 50\,Hz$ respectively are lowered by using a higher cathode stoichiometry, and such a variation is more pronounced for the process at $\sim 10\,Hz$. Both processes are correlated with the oxygen reduction occurring at the cathode. The charge transfer kinetics of the ORR are described by the Butler-Volmer equation (Eq. (7)).

$$i = i_0 \left\{ \exp\left(\frac{\alpha z F \eta}{RT}\right) - \exp\left[-\frac{(1-\alpha) z F \eta}{RT}\right] \right\} \tag{7}$$

Using the inverse slope of the Butler-Volmer curve at the studied operation point, the corresponding resistance R_{CT} is calculated (Eq. (8)) [59].

$$R_{CT} = \frac{\partial \eta}{\partial i} \tag{8}$$

Fig. 6. Final assignment of the peaks and representation of the single contributions of each process. The example is based on Impedance (a) and DRT plot (b) obtained during HT-PEMFC operation at $T = 160\,°C$, $j = 300\,mA\,cm^{-2}$, $\lambda_{H2} = 1.8$, $\lambda_{Air} = 2.5$.

Varying λ_{Air} causes a change in partial pressure of oxygen (p_{O2}), thereby altering the exchange current density and consequently the Butler-Volmer curve [60]. Accordingly modifying the cathode stoichiometry amends the resistance correlated with the oxygen reduction reaction.

The adjacent peaks at high frequencies (**P4–P7**) are not affected at all by a variation of λ_{air} and thus assumed to be related to anode processes, such as the charge transfer kinetics of the hydrogen oxidation reaction (HOR) or proton conduction related processes. These results are in good agreement with the previous assignment of the individual features and prove the reliability of the DRT approach for studying the effects of various fuel cell parameters.

3.3.2. Current density

The impact of current was investigated and impedance was measured at different current densities, whereas temperature ($T = 160\,°C$) and stoichiometry ($\lambda_{Air} = 2.5/\lambda_{H2} = 1.8$) were kept constant (Fig. 8).

During current variation the cell operation point is shifted along the polarization curve (Fig. 8a). In the Nyquist plot (Fig. 8b) the low frequency part of the impedance shrinks, but the contributions of kinetics and mass transport are not separable.

The distribution functions (Fig. 8c) show the changes more intuitively. Therein, P1 stays nearly constant whereas **P2–P3** are affected by the current variation [53]. The reason why mass transport is not altered can be related to the current range in this set of experiments. According to Fig. 8a), $j = 500\,mA\,cm^{-2}$ is still in a region where the polarization curve is dominated by activation and ohmic losses. For this reason, a limitation by mass transport seems unlikely.

Both **P2** and **P3** have been associated with the oxygen reduction reaction. During a current variation both are reduced and slightly accelerated. The trend is progressive and indicates that kinetic losses decrease with increasing current density, which is explained by the Butler-Volmer equation [59,60]. These dependencies are in good agreement with the assignments, and the system behavior is expected [9].

The broad feature **P4** and the adjacent peaks (**P5–P7**) are slightly altered by varying the current. These peaks are assumed to represent the anode side, but with the limited measurements we have so far the underlying process is not yet identified.

These results indicate that the DRT technique can successfully detect changes in cell internal losses that are induced by current density variation. The assignments of **P1** to mass transport and **P2**

and **P3** to oxygen reduction reaction related processes are confirmed within the current and stoichiometry variation.

4. Conclusion

In this study, the distribution of relaxation times (DRT) was applied successfully to analyze impedance spectra of a high-temperature PEM fuel cell doped with phosphoric acid. To the authors' knowledge, this study represents the first application of the DRT approach to a polymer fuel cell. Up to seven peaks were visible in the DRT distribution function, whereas only three distinguishable features were observed in the Nyquist plot. DRT shows distinct peaks around well-defined frequencies. A specific set of experimental conditions (cell operation in H_2/Air and H_2/O_2, hydrogen pumping, j and λ_{Air} variations) were chosen to identify the features in the DRT function with the cell's internal phenomena without ambiguity. While mass transport is identified as the cause of the peak around 1 Hz, ORR appears to have contributed to two main peaks located at 10 Hz and 50 Hz, and features above 1 kHz are attributed to anode and proton conduction mechanisms.

This work demonstrates DRT as a suitable technique for the study of HT-PEMFCs impedance, especially with new experimental conditions for which little a-priori knowledge about the underlying system is available. With DRT, unambiguous identification of polarization losses based on their respective time constants is possible. This method has significant advantages in terms of high precision and low computational cost. DRT can be applied in combination with ECM or physical models, since it can deliver useful information for the development of those techniques and models.

References

[1] J.T. Wang, R.F. Savinell, J. Wainright, M. Litt, H. Yu, A H2O2 fuel cell using acid doped polybenzimidazole as polymer electrolyte, Electrochimica Acta 41 (1996) 193–197.
[2] S.S. Araya, F. Zhou, V. Liso, S.L. Sahlin, J.R. Vang, S. Thomas, X. Gao, C. Jeppesen, S.K. Kær, A comprehensive review of PBI-based high temperature PEM fuel cells, International Journal of Hydrogen Energy 41 (2016) 21310–21344.
[3] R. Zeis, Materials and characterization techniques for high-temperature polymer electrolyte membrane fuel cells, Beilstein journal of nanotechnology 6 (2015) 68–83.
[4] Q. Li, R. He, J.O. Jensen, N.J. Bjerrum, PBI-Based Polymer Membranes for High Temperature Fuel Cells –Preparation, Characterization and Fuel Cell Demonstration, Fuel Cells 4 (2004) 147–159.
[5] M.E. Orazem, B. Tribollet, Electrochemical impedance spectroscopy, Wiley, Hoboken, N.J, 2008.
[6] S.M. Rezaei Niya, M. Hoorfar, Study of proton exchange membrane fuel cells using electrochemical impedance spectroscopy technique – A review, Journal of Power Sources 240 (2013) 281–293.
[7] T.E. Springer, T.A. Zawodzinski, M.S. Wilson, S. Gottesfeld, Characterization of Polymer Electrolyte Fuel Cells Using AC Impedance Spectroscopy, Journal of The Electrochemical Society 143 (1996) 587–599.
[8] X. Yuan, H. Wang, J. Colin Sun, J. Zhang, AC impedance technique in PEM fuel cell diagnosis—A review, International Journal of Hydrogen Energy 32 (2007) 4365–4380.
[9] J.L. Jespersen, E. Schaltz, S.K. Kær, Electrochemical characterization of a polybenzimidazole-based high temperature proton exchange membrane unit cell, Journal of Power Sources 191 (2009) 289–296.
[10] F. Mack, R. Laukenmann, S. Galbiati, J.A. Kerres, R. Zeis, Electrochemical Impedance Spectroscopy as a Diagnostic Tool for High-Temperature PEM Fuel Cells, ECS Transactions 69 (2015) 1075–1087.
[11] M. Mamlouk, K. Scott, Analysis of high temperature polymer electrolyte membrane fuel cell electrodes using electrochemical impedance spectroscopy, Electrochimica Acta 56 (2011) 5493–5512.
[12] R. Petrone, Z. Zheng, D. Hissel, M.C. Péra, C. Pianese, M. Sorrentino, M. Becherif, N. Yousfi-Steiner, A review on model-based diagnosis methodologies for PEMFCs, International Journal of Hydrogen Energy 38 (2013) 7077–7091.
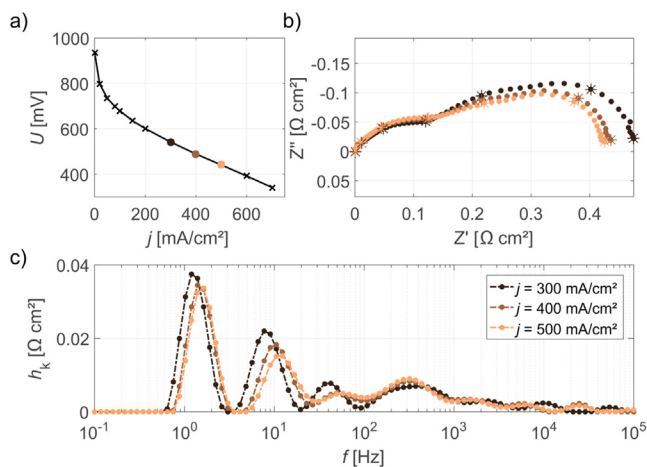
Fig. 8. Impact of current density variation on HT-PEMFC polarization losses. (a) Polarization curves, (b) impedance and 4 (c) DRT plots at different current densities ($T = 160\,°C$, $\lambda_{H2}2 = 1.8$, $\lambda_{Air}i = 2.5$).

[13] X.-Z.R. Yuan, C. Song, H. Wang, J. Zhang, Electrochemical impedance spectroscopy in PEM fuel cells: fundamentals and applications, Springer Science & Business Media, 2009.

[14] M. Boaventura, A. Mendes, Activation procedures characterization of MEA based on phosphoric acid doped PBI membranes, International Journal of Hydrogen Energy 35 (2010) 11649–11660.

[15] S. Galbiati, A. Baricci, A. Casalegno, G. Carcassola, R. Marchesi, On the activation of polybenzimidazole-based membrane electrode assemblies doped with phosphoric acid, International Journal of Hydrogen Energy 37 (2012) 14475–14481.

[16] J.R. Vang, S.J. Andreasen, S.S. Araya, S.K. Kær, Comparative study of the break in process of post doped and sol-gel high temperature proton exchange membrane fuel cells, International Journal of Hydrogen Energy 39 (2014) 14959–14968.

[17] W. Maier, T. Arlt, K. Wippermann, C. Wannek, I. Manke, W. Lehnert, D. Stolten, Correlation of Synchrotron X-ray Radiography and Electrochemical Impedance Spectroscopy for the Investigation of HT-PEFCs, Journal of The Electrochemical Society 159 (2012) F398–F404.

[18] C.-Y. Chen, W.-H. Lai, Effects of temperature and humidity on the cell performance and resistance of a phosphoric acid doped polybenzimidazole fuel cell, Journal of Power Sources 195 (2010) 7152–7159.

[19] K. Wippermann, C. Wannek, H.F. Oetjen, J. Mergel, W. Lehnert, Cell resistances of poly(2,5-benzimidazole)-based high temperature polymer membrane fuel cell membrane electrode assemblies: Time dependence and influence of operating parameters, Journal of Power Sources 195 (2010) 2806–2809.

[20] J. Lobato, P. Cañizares, M.A. Rodrigo, J.J. Linares, F.J. Pinar, Study of the influence of the amount of PBI–H3PO4 in the catalytic layer of a high temperature PEMFC, International Journal of Hydrogen Energy 35 (2010) 1347–1355.

[21] M.S. Kondratenko, M.O. Gallyamov, A.R. Khokhlov, Performance of high temperature fuel cells with different types of PBI membranes as analysed by impedance spectroscopy, International Journal of Hydrogen Energy 37 (2012) 2596–2602.

[22] J. Parrondo, C. Venkateswara Rao, S.L. Ghatty, B. Rambabu, Electrochemical Performance Measurements of PBI-Based High-Temperature PEMFCs, International Journal of Electrochemistry 2011 (2011) 8.

[23] F. Mack, T. Morawietz, R. Hiesgen, D. Kramer, V. Gogel, R. Zeis, Influence of the polytetrafluoroethylene content on the performance of high-temperature polymer electrolyte membrane fuel cell electrodes, International Journal of Hydrogen Energy 41 (2016) 7475–7483.

[24] S. Kaserer, C. Rakousky, J. Melke, C. Roth, Design of a reference electrode for high-temperature PEM fuel cells, Journal of Applied Electrochemistry 43 (2013) 1069–1078.

[25] S.J. Andreasen, J.R. Vang, S.K. Kær, High temperature PEM fuel cell performance characterisation with CO and CO 2 using electrochemical impedance spectroscopy, International journal of hydrogen energy 36 (2011) 9815–9830.

[26] S. Araya, S. Andreasen, S. Kær, Experimental Characterization of the Poisoning Effects of Methanol-Based Reformate Impurities on a PBI-Based High Temperature PEM Fuel Cell, Energies 5 (2012) 4251.

[27] M. Boaventura, I. Alves, P. Ribeirinha, A. Mendes, The influence of impurities in high temperature polymer electrolyte membrane fuel cells performance, International Journal of Hydrogen Energy 41 (2016) 19771–19780.

[28] M. Boaventura, H. Sander, K.A. Friedrich, A. Mendes, The influence of CO on the current density distribution of high temperature polymer electrolyte membrane fuel cells, Electrochimica Acta 56 (2011) 9467–9475.

[29] F. Zhou, S.J. Andreasen, S.K. Kær, J.O. Park, Experimental investigation of carbon monoxide poisoning effect on a PBI/H3PO4 high temperature polymer electrolyte membrane fuel cell: Influence of anode humidification and carbon dioxide, International Journal of Hydrogen Energy 40 (2015) 14932–14941.

[30] S. Simon Araya, S. Juhl Andreasen, H. Venstrup Nielsen, S. Knudsen Kær, Investigating the effects of methanol-water vapor mixture on a PBI-based high temperature PEM fuel cell, International Journal of Hydrogen Energy 37 (2012) 18231–18242.

[31] F.J. Pinar, N. Pilinski, M. Rastedt, P. Wagner, Performance of a high-temperature PEM fuel cell operated with oxygen enriched cathode air and hydrogen from synthetic reformate, International Journal of Hydrogen Energy 40 (2015) 5432–5438.

[32] F.J. Pinar, N. Pilinski, P. Wagner, Long-term testing of a high temperature polymer electrolyte membrane fuel cell: The effect of reactant gases, AIChE Journal 62 (2016) 217–227.

[33] S. Galbiati, A. Baricci, A. Casalegno, R. Marchesi, Degradation in phosphoric acid doped polymer fuel cells: A 6000 h parametric investigation, International Journal of Hydrogen Energy 38 (2013) 6469–6480.

[34] J.-R. Kim, J.S. Yi, T.-W. Song, Investigation of degradation mechanisms of a high-temperature polymer-electrolyte-membrane fuel cell stack by electrochemical impedance spectroscopy, Journal of Power Sources 220 (2012) 54–64.

[35] J. Lobato, P. Canizares, M.A. Rodrigo, J.J. Linares, PBI-based polymer electrolyte membranes fuel cells: Temperature effects on cell performance and catalyst stability, Electrochimica acta 52 (2007) 3910–3920.

[36] F. Zhou, S. Simon Araya, I. Florentina Grigoras, S. Juhl Andreasen, S. Knudsen Kær, Performance Degradation Tests of Phosphoric Acid Doped Polybenzimidazole Membrane Based High Temperature Polymer Electrolyte Membrane Fuel Cells, Journal of Fuel Cell Science and Technology 12 (2015) 021002–021002.

[37] A. Baricci, M. Zago, A. Casalegno, A Quasi 2D Model of a High Temperature Polymer Fuel Cell for the Interpretation of Impedance Spectra, Fuel Cells 14 (2014) 926–937.

[38] C. Bao, W.G. Bessler, Two-dimensional modeling of a polymer electrolyte membrane fuel cell with long flow channel. Part I. Model development, Journal of Power Sources 275 (2015) 922–934.

[39] A.M. Dhirde, N.V. Dale, H. Salehfar, M.D. Mann, T.H. Han, Equivalent Electric Circuit Modeling and Performance Analysis of a PEM Fuel Cell Stack Using Impedance Spectroscopy, IEEE Transactions on Energy Conversion 25 (2010) 778–786.

[40] A. Leonide, V. Sonn, A. Weber, E. Ivers-Tiffée, Evaluation and Modeling of the Cell Resistance in Anode-Supported Solid Oxide Fuel Cells, Journal of The Electrochemical Society 155 (2008) B36–B41.

[41] J.P. Schmidt, T. Chrobak, M. Ender, J. Illig, D. Klotz, E. Ivers-Tiffée, Studies on LiFePO4 as cathode material using impedance spectroscopy, Journal of Power Sources 196 (2011) 5342–5348.

[42] M.A. Danzer, M. Petzl, Voltage and impedance analysis for the indirect detection and characterization of lithium plating in commercial LFP/graphite Li-ion cells, ECS Poster, 17th International Meeting on Lithium Batteries (IMLB 2014), Como, Italy, June 10–14, 2014.

[43] H. Schichlein, A.C. Müller, M. Voigts, A. Krügel, E. Ivers-Tiffée, Deconvolution of electrochemical impedance spectra for the identification of electrode reaction mechanisms in solid oxide fuel cells, Journal of Applied Electrochemistry 32 (2002) 875–882.

[44] T. Steenberg, H.A. Hjuler, C. Terkelsen, M.T. Sánchez, L.N. Cleemann, F.C. Krebs, Roll-to-roll coated PBI membranes for high temperature PEM fuel cells, Energy & Environmental Science 5 (2012) 6076–6080.

[45] F. Mack, S. Heissler, R. Laukenmann, R. Zeis, Phosphoric acid distribution and its impact on the performance of polybenzimidazole membranes, Journal of Power Sources 270 (2014) 627–633.

[46] F. Mack, M. Klages, J. Scholta, L. Jörissen, T. Morawietz, R. Hiesgen, D. Kramer, R. Zeis, Morphology studies on high-temperature polymer electrolyte membrane fuel cell electrodes, Journal of Power Sources 255 (2014) 431–438.

[47] F. Mack, T. Morawietz, R. Hiesgen, D. Kramer, R. Zeis, PTFE Distribution in High-Temperature PEM Electrodes and Its Effect on the Cell Performance, ECS Transactions 58 (2013) 881–888.

[48] A. Huth, B. Schaar, T. Oekermann, A proton pump concept for the investigation of proton transport and anode kinetics in proton exchange membrane fuel cells, Electrochimica Acta 54 (2009) 2774–2780.

[49] B.A. Boukamp, A Linear Kronig-Kramers Transform Test for Immittance Data Validation, Journal of The Electrochemical Society 142 (1995) 1885–1894.

[50] E. Barsoukov, J.R. Macdonald, Impedance spectroscopy: theory, experiment, and applications, John Wiley & Sons, 2005.

[51] A.N. Tikhonov, A. Goncharsky, V. Stepanov, A.G. Yagola, Numerical methods for the solution of ill-posed problems, Springer Science & Business Media, 2013.

[52] J. Weese, A reliable and fast method for the solution of Fredhol integral equations of the first kind based on Tikhonov regularization, Computer Physics Communications 69 (1992) 99–111.

[53] S. Schindler, A. Weiß, S. Galbiati, F. Mack, M.A. Danzer, R. Zeis, Identification of Polarization Losses in High-Temperature PEM Fuel Cells by Distribution of Relaxation Times Analysis, ECS Transactions 75 (2016) 45–53.

[54] V.A. Paganin, C.L.F. Oliveira, E.A. Ticianelli, T.E. Springer, E.R. Gonzalez, Modelisticinterpretation of the impedance response of a polymer electrolyte fuel cell1, Electrochimica Acta 43 (1998) 3761–3766.

[55] T.J. Schmidt, J. Baurmeister, Properties of high-temperature PEFC Celtec®-P 1000 MEAs in start/stop operation mode, Journal of Power Sources 176 (2008) 428–434.

[56] I.A. Schneider, M.H. Bayer, S. von Dahlen, Locally Resolved Electrochemical Impedance Spectroscopy in Channel and Land Areas of a Differential Polymer Electrolyte Fuel Cell, Journal of The Electrochemical Society 158 (2011) B343–B348.

[57] M. Markiewicz, C. Zalitis, A. Kucernak, Performance measurements and modelling of the ORR on fuel cell electrocatalysts – the modified double trap model, Electrochimica acta 179 (2015) 126–136.

[58] S. Kaserer, K.M. Caldwell, D.E. Ramaker, C. Roth, Analyzing the Influence of H3PO4 as Catalyst Poison in High Temperature PEM Fuel Cells Using in-operando X-ray Absorption Spectroscopy, The Journal of Physical Chemistry C 117 (2013) 6210–6217.

[59] R. O'Hayre, S.W. Cha, W. Colella, F.B. Prinz, Fuel cell reaction kinetics, Fuel cell fundamentals (2006) 77–116.

[60] A. Bard, L. Faulkner, Electrochemical Methods: Fundamentals and Applications, Johnwiley & Sons, Inc, New York, 2001.